https://doi.org/10.1016/j.cej.2024.148727

Revised Ms. CEJ-D-23-27993

(Original Research Article)

Developing novel high-performance polyethylene-embedded phase change emulsions with minimal supercooling for efficient thermal energy storage

Liu Liu [a, b], Jian Yong Wu [a, *]

[a] Department of Food Science and Nutrition, The Hong Kong Polytechnic University, Hung Hom, Kowloon, Hong Kong SAR, China

[b] Liangjiang International College, Chongqing University of Technology, Chongqing, 400054, China

[*] Corresponding author:

E-mail address: jian-yong.wu@polyu.edu.hk (J.Y. Wu).

ABSTRACT

Phase change emulsions are promising thermal fluids, but have been frustrated by high degrees of supercooling. The existing methods for supercooling reduction involve the addition of various nucleating agents (NAs) but achieve limited success due to a lack of commonality and negative impact on emulsion stability. This study explored a strategy by integrating interface-induced and NA-induced nucleation. A diblock copolymer was positioned at the interface, and a new NA, polyethylene, was efficiently embedded into the droplets assisted by ultrasonication to minimize supercooling and extend stability. Firstly, hexadecane emulsion was chosen for assessment of the chemical compositions and ultrasonication conditions. A higher ultrasound intensity facilitated the polyethylene embedment, providing sufficient nucleation sites within the droplets with a low mass content (1%). The functionality of polyethylene was found to be size-dependent, resulting in a single melting/freezing peak and a low supercooling degree (ΔT) of 3.7 ℃ for hexadecane droplets of 256.3 nm average diameter. Subsequently, the effectiveness of polyethylene was evaluated on other seven paraffin emulsions with higher melting points (T_m), achieving minimal supercooling (ΔT = 0.2-2.6 ℃). Furthermore, dynamic stability was evaluated by applying an emulsion template ($T_m \approx 54$ ℃) to a rig for long period and repeated thermal cycles (6 months and 9000 cycles). The average diameter increased marginally from 374.1 to 393.4 nm, while the ΔT remained stable at 2.5 ℃, and the latent heat slightly decreased. No obvious sign of emulsion breakdown was observed during an additional six-month storage period. An effective strategy has been developed for formulating a range of novel phase change emulsions with extended service life and minimal supercooling which are desirable for thermal energy storage applications.

Keywords: Phase change emulsion; supercooling elimination; ultrasonication; thermal cycles; dynamic stability.

Nomenclature

ΔH	latent heat, J/g
T	temperature, ℃
ΔT	supercooling degree, ℃

Subscripts	
f	freezing
m	melting
o	onset
p	peak
Abbreviations	
C16	hexadecane
C24	tetracosane
C28	octacosane
C32	dotriacontane
DLS	dynamic light scattering
DSC	differential scanning calorimetry
NA	nucleating agent
PCE	phase change emulsion
PCM	phase change material
PCS	phase change slurry
PDI	polydispersity index
PE	polyethylene
PE-b-PEG	polyethylene-block-poly(ethylene glycol)
PIT	phase inversion point
Sal52	Sasolwax 5203
SEM	scanning electron microscopy
TES	thermal energy storage

1. Introduction

Phase change materials (PCMs) are the essential media for thermal energy storage (TES) techniques to store latent heat across low [1], intermediate [2], and high temperature ranges [3], which can be applied in thermal management and various energy conversion systems such as solar-thermal and solar-thermal-electric units [4]. Considerable research effort has been made to developing composite PCMs because of their unique characteristics. Among one the most preferable PCM composites are PCM capsules which are fabricated by coating PCM with a continuous shell material, thereby forming individual PCM capsules at the nanoscale [5] and microscale [6]. This technique may prevent leakage and corrosion during PCM melting, enhance heat transfer by increasing the specific surface area, and also impart special properties through the capsule shell, such as high photothermal conversion efficiency [7]. PCM capsules can also be dispersed in a carrier fluid to form phase change slurries (PCSs) [8], which absorb

more thermal energy of latent heat within the phase transition temperature range than the conventional heat transfer fluids. As a result, PCSs have found versatile applications in geothermal energy [9], solar energy harvesting [10], and thermal management for Li-ion batteries [11], photovoltaic cells [12], fuel cells [13], and light-emitting diodes [14].

However, the technique for fabrication of PCM capsules is rather intricate and time-consuming, involving multiple steps including emulsion template formation, polymerization, washing, and drying [15-17]. Another major drawback is the high degree of supercooling, preventing the PCM core from solidifying at the desired cooling temperature for latent heat storage. Increasing the capsule size can partially alleviate supercooling [18] but greatly reduce the heat transfer area and mechanical stability. Although ingenious approaches have been attempted to manipulate the morphology and roughness of capsule shell to induce PCM nucleation [19], the most common and feasible strategy for reducing supercooling of PCM capsules is the embedding of nucleating agents (NAs) within the PCM core. Qiu et al. [20] introduced graphene quantum dots and nano-Al_2O_3 into paraffin capsules, where the former completely eliminated supercooling but the latter had no effect. Alternatively, organic NAs such as hexadecanol [21] have been explored but not effectively minimize supercooling.

Phase change emulsions (PCEs), which were initially prepared as the emulsion template for PCM capsules, have emerged as a promising alternative to PCSs [22], owning to a much simpler fabrication process and a versatile role in thermal management for photovoltaic cells [23] and Li-ion batteries [24]. To compensate for their thermodynamically unstable nature, PCEs are prepared in smaller droplet size than PCSs to prolong the duration before destabilization occurs. Various techniques, including high-energy devices such as high-pressure homogenizers [25] and ultrasonicators [26] and low-energy methods such as D-phase [27] and phase inversion temperature (PIT) [28], have enabled the production of PCE droplets at the nanoscale. However, supercooling is often more pronounced in PCEs than PCSs [29]. In essence, PCEs retain their excellent stability at the expense of high supercooling.

Considering the influence of emulsifiers present at the interface between droplets and water on supercooling, researchers have explored the use of emulsifiers such as diblock

copolymers [28], polyvinyl alcohols [30], and high-melting fats [31] to modulate nucleation. As the use of these unconventional emulsifiers alone has been found insufficient, the addition of NAs is still the primary approach for supercooling suppression in PCEs. Multi-walled carbon nanotubes were found effective to reduce supercooling in a hexadecane emulsion [32] but not on octadecane emulsions [26]. Barison et al. [33] studied the impact of graphene oxide on the thermal properties of two paraffin emulsions, showing significance only for one of them. High-melting paraffins [28, 34] used as NAs also encountered the challenges in effectively minimize supercooling entailing the need for novel NAs and innovative strategies that can be applied to various PCEs. Moreover, the degree of supercooling in PCEs could be aggravated by circulation through pipes during repeated heating-cooling cycles. For instance a previous study [35] found that the supercooling degree of a PCE was increased from 2.8 ℃ initially to over 10 ℃ after 70 days of operation, resulting in lower energy storage capacity. Another study [36] also observed that PCEs with significant supercooling exhibited poorer thermal management performance for photovoltaic modules compared to water. Therefore, it is crucial to maintain both high emulsion stability and low supercooling over long-term operation for the practical application of PCEs.

To overcome the technical barrier to achieving both a high emulsion stability and a low supercooling of PCEs, this work was to investigate a novel strategy by combining synergistically interface-induced and NA-induced heterogeneous nucleation. Specifically, a diblock copolymer, polyethylene-block-poly(ethylene glycol) and polyethylene were chosen based on previous studies [28, 37] and used for nucleation at the interface and in the core of PCEs, respectively. Ultrasonication was applied to facilitate the embedding of polyethylene within small PCE droplets. The ultrasonication conditions and chemical compositions were assessed for a hexadecane emulsion and then applied for several other paraffin emulsions with higher melting points (T_m) up to 70 ℃. A representative paraffin emulsion with a T_m of about 54 ℃ was pumped through a testing rig for six months, underdoing a total of 9000 thermal cycles, followed by storage for an additional six months. The potential of the proposed strategy was demonstrated for practical applications in formulating high-performance PCEs covering a

T_m range from 20 to 70 ℃.

2. Materials and methods

2.1 Materials

N-alkanes, including hexadecane (C16, purity: 98.0%), tetracosane (C24, purity: 99.0%), octacosane (C28, purity: 98.0%), and dotriacontane (C32, purity: 96.0%), were procured from Tokyo Chemical Industry. Commercial PCMs (OP28E, OP44E and OP65E) were sourced from Hangzhou Ruhr Tech Co., Ltd. Paraffin Sasolwax 5203, denoted as Sal52, was provided by Sasol Wax GmbH. Nonionic surfactants, Brij L4 and Cremophor® A25, were acquired from Sigma-Aldrich. A diblock copolymer, polyethylene-block-poly(ethylene glycol) (PE-*b*-PEG) with a number average molecular weight of about 2250, and polyethylene (PE) with a number average molecular weight of around 1700, were also obtained from Sigma-Aldrich. All chemicals were used without further treatment.

2.2 Preparation of PCEs

A binary surfactant system composed of Brij L4 to Cremophor® A25 in a mass ratio of 7:3 [37] was employed to stabilize a two-phase colloidal system. The fabrication process of 20% PCEs is briefly outlined in **Fig. 1**. Initially, 4 g of PCM was mixed with Brij L4 and any required additives, followed by stirring at 400 rpm and 90 ℃ to achieve a homogeneous oil phase. Next, Cremophor® A25 was dissolved in distilled water at 300 rpm and 80 ℃, and the heated aqueous phase was introduced to the oil phase at a rate of 10 mL/min. The resulting emulsion with a mass of 20 g was subsequently cooled to room temperature and transferred to a 50 mL beaker for further emulsification using a sonicator (VCX 750, Sonics & Materials) fitted with a 13 mm probe having a constant frequency of 20 kHz and a maximum power of 750 W. The ultrasound pulse ON/OFF cycle was set to 30/30 s, and the beaker was cooled in an ice-water bath during the ultrasonication process.

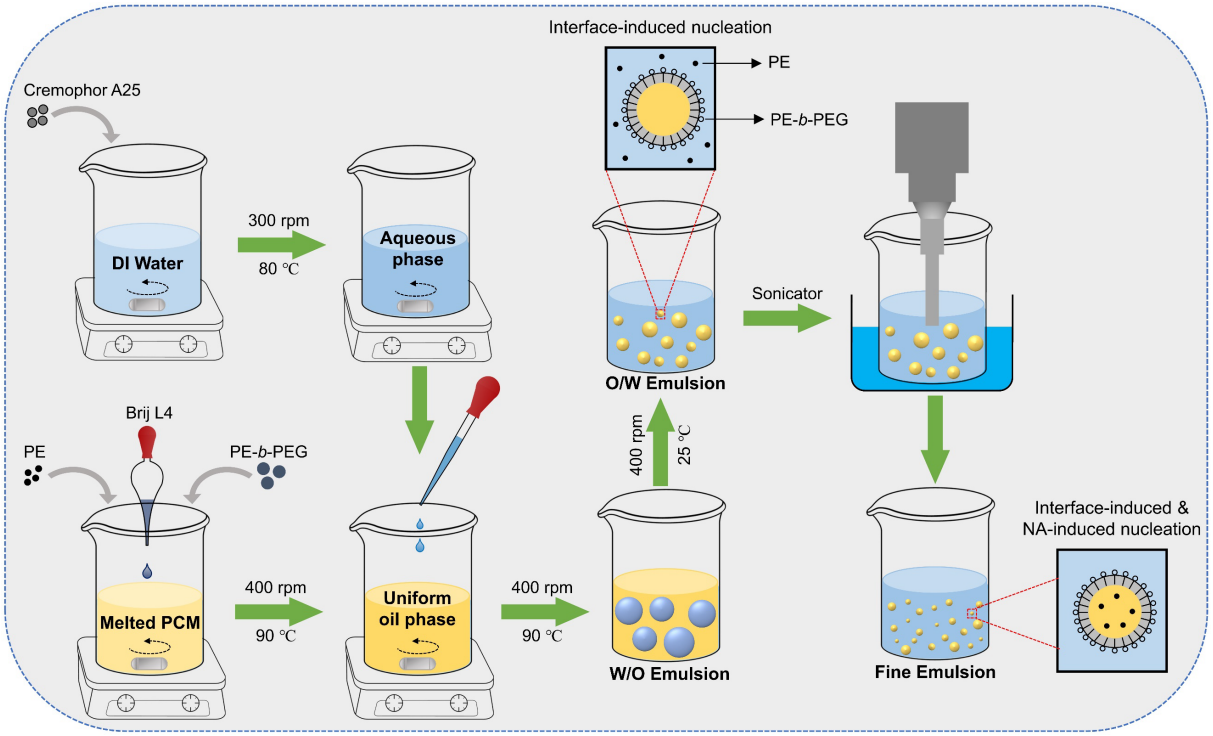

Fig. 1 Schematic of 20% PCEs preparation with melting point (T_m) ranging from 20 to 70 ℃.

Notably, with a high surfactant content, a phase inversion occurred as the emulsion was cooled, transitioning from water-in-oil (W/O) to oil-in-water (O/W). This phenomenon was in accordance with the procedures of the PIT method [37]. In this stage, it was difficult for PE to be entrapped into the droplets due to the low energy input during emulsification, resulting in a visible layer of unencapsulated NA floating on the surface of the PCEs. Subsequent high-energy ultrasound would enhance the efficient embedding of PE into the droplets through the transient cavitation effect, leading to the disappearance of the macroscopic PE layer. However, the droplet size would increase to some extent because ultrasonic emulsification is less effective than the PIT method in reducing droplet size when the surfactant content is high. The nucleation of PCM could be induced at the interface and in the droplets by PE. If the surfactant concentration decreased, the PIT method would be ineffective during cooling. In such cases, ultrasonication would be responsible for droplet size reduction and PE entrapment.

The influence of ultrasound amplitude, treatment duration, and chemical composition on the supercooling of PCEs was thoroughly examined using the C16 emulsion, as summarized in **Table 1**. The optimal chemical compositions and formulation conditions determined for the C16 emulsion were subsequently applied to a range of paraffin emulsions with higher melting

points to assess the effectiveness of this proposed strategy for suppressing supercooling in PCEs. Furthermore, a commercial paraffin Sal52 with a relatively high melting point (T_m = 53.4 °C) was chosen as an example in the following evaluation, as it is cost-effective and a high heating temperature for PCE melting can accelerate the emulsion breakdown compared to low-melting PCEs. Approximately 1 L Sal52 emulsion was produced and tested in a rig for six months, to monitor variations in supercooling degree, droplet size, and latent heat. An additional six months of storage at room temperature was performed to observe any destabilization phenomenon, thereby evaluating the service life of the developed PCE.

Table 1 Essential experimental variables for suppressing supercooling in 20% PCEs (All % values in weight% for emulsion composition).

PCM	Surfactant content	PE-*b*-PEG	PE	Amplitude	Time
C16	10%	None or 2%	None or 1%	75%	5 min
C16	10%	2%	1%	75-100%	1-5 min
C16	10%	2%	0.5-2%	100%	5 min
C16	2-10%	2%	1%	100%	5-15 min
C16	2%	2%	1-3%	100%	10 min
Varies	2%	2%	1%	100%	10 min

2.3 Characterization of PCEs

The Z-average droplet diameter and polydispersity index (PDI) of PCEs were measured using dynamic light scattering (DLS) with a Malvern Zetasizer Nano ZS. For measurements, each PCE was diluted 200-fold, and triplicate measurements of 15 runs were conducted at 25 °C. Morphology of PCEs was observed using scanning electron microscopy (SEM) with a TESCAN MIRA instrument. To prepare samples for SEM analysis, PCEs were diluted 1000-fold in distilled water, and a small sample drop was spread onto a silicon substrate surface and dried at room temperature. The apparent viscosity of PCEs at a shear rate of around 6 s^{-1} was measured three times using a rotational viscometer (Brookfield, DV3T) at room temperature around 22 °C. The thermal properties of PCEs were determined using a differential scanning calorimeter (Mettler Toledo, DSC3) at a scanning rate of 5 °C/min in a nitrogen atmosphere.

The supercooling degree (ΔT) was calculated by determining the difference between the onset melting ($T_{m,o}$) and freezing points ($T_{f,o}$), which were independent of the scanning rate [38]. The peak points of melting ($T_{m,p}$) and freezing ($T_{f,p}$) were employed to indicate the melting and freezing peaks.

3. Results and discussion

3.1 Characterization of C16 emulsion

3.1.1 Effects of chemical compositions and ultrasonic conditions on supercooling

A 20% C16 emulsion stabilized by 10% surfactants (referred to the bare emulsion) was subjected to ultrasound at 75% amplitude for 5 minutes. Subsequently, PE-*b*-PEG and PE were added either individually or in combination. The freezing and melting behaviors of the resulting emulsions were analyzed using DSC, with the observed curves shown in **Fig. 2a-b**. The bare emulsion displayed a high degree of supercooling ($\Delta T \approx 9$ ℃) and a single freezing peak at a freezing point ($T_{f,p}$) of 3 ℃. The single freezing peak with a much lower T_f was primarily attributed to the homogeneous nucleation of confined C16 within the droplets [39], which was consistent with previous studies with no nucleating agents [27, 28, 40]. Adding 2% PE-*b*-PEG somewhat facilitated C16 nucleation, potentially via an interface-induced heterogeneous nucleation [28], resulting in a new freezing peak with a $T_{f,p}$ of 10 ℃ and a slight shift of the main freezing peak. However, the latent heat proportion was minimal, and increasing PE-*b*-PEG concentrations did not raise its proportion but significantly increased emulsion viscosity. Incorporating 1% PE produced a comparable peak with a slightly higher $T_{f,p}$ and latent heat proportion. The initial freezing peak ($T_{f,p}$ = 3 ℃) split into two peaks upon adding PE, with the new peak at a $T_{f,p}$ of 6.5 ℃ became the primary freezing peak when combining PE-*b*-PEG and PE, involving interface-induced and NA-induced nucleation. The presence of multiple freezing peaks could be attributed to the uneven distribution of PE within the C16 droplets, and further optimization of the preparation conditions is needed to improve the entrapment of PE.

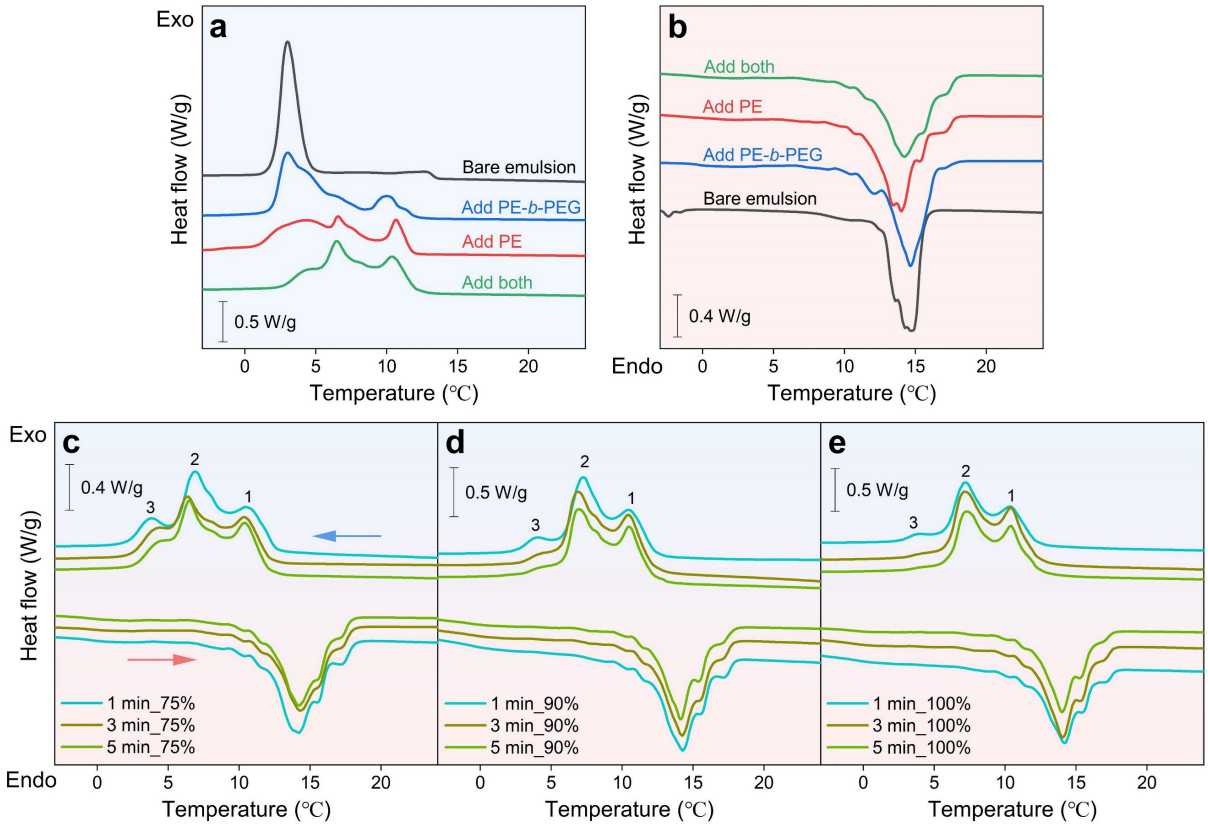

Fig. 2 DSC curves of 20% C16 emulsion with 10% surfactants: (a-b) freezing and melting process upon adding PE-*b*-PEG and/or PE, combined with ultrasound at 75% amplitude for 5 min; (c-e) ultrasound at 75-100% amplitude for 1-5 min, accompanied by the addition of 2% PE-*b*-PEG and 1% PE.

The ultrasonic conditions were then adjusted to optimize the DSC freezing curves in the presence of PE-*b*-PEG and PE, and the corresponding DSC curves are depicted in **Fig. 2c-e**. It was observed that at 75% amplitude, extending the ultrasound treatment duration led to a slight reduction in the third freezing peak. This reduction was further intensified at 90% amplitude, and the third freezing peak disappeared entirely at 100% amplitude for 5 minutes, suggesting that higher energy input effectively trapped PE within C16 droplets. Importantly, the presence of a single freezing peak (the 1st) was considered ideal, as it indicated complete elimination of supercooling. Therefore, adjusting the concentration of PE may achieve this goal, causing the 2nd freezing peak to vanish.

3.1.2 Effect of PE concentration on supercooling

The influence of PE concentration (0.5-2%) on the properties of a 20% C16 emulsion with

2% PE-*b*-PEG and 10% surfactants was examined. Firstly, the changes in the phase change point of bulk C16 with the addition of different PE masses are summarized in **Table 2**, and the corresponding DSC curves can be found in **Fig. S1** (Supplementary data). Adding PE to bulk C16 at a 2.0/20 mass ratio resulted in a decrease of about 1 ℃ in both melting and freezing points, while ΔT remained constant at a low value of 1.6 ℃.

Table 2 Impact of PE on melting and freezing points of bulk C16.

PE/C16 mass ratio	$T_{m,o}$ (℃)	$T_{m,p}$ (℃)	$T_{f,o}$ (℃)	$T_{f,p}$ (℃)	ΔT (℃)
0	17.5	19.9	15.9	15.9	1.6
0.5/20	17.3	19.5	15.7	15.5	1.6
1.0/20	17.1	18.7	15.7	15.6	1.4
1.5/20	16.9	18.5	15.3	15.2	1.6
2.0/20	16.6	18.5	14.9	14.9	1.7

Fig. 3 demonstrates the impact of PE concentration on the properties of C16 emulsion under fixed ultrasonic conditions of 100% amplitude and 5 minutes. It was found that the concentration-dependent effect of PE on the DSC freezing/melting curve change was minimal. Specifically, 1% PE may provide sufficient sites for heterogeneous nucleation, and C16 crystallization process would still be dominated by the small droplet volume. In other words, intentionally increasing droplet size could potentially shift the primary freezing peak, but caution must be exercised to prevent emulsion instability. Furthermore, the addition of PE exhibited limited negative effects on the apparent viscosity and droplet size of the C16 emulsion. The apparent viscosity of the C16 emulsion increased from 67.7 mPa·s to 73.9 mPa·s with the addition of 1% PE, as illustrated in **Fig. 3b**. It then rose by about 50% when the PE content was increased to 2%. A monomodal droplet size distribution was observed for any PE concentration (**Fig. 3c**), with negligible changes in the distribution upper/lower limits. As a result, the average diameter and PDI were marginally increased to 107.7 nm and 0.20, respectively, with 2% PE, compared to 96.4 nm and 0.18 without PE (**Fig. 3d**). These results suggest that the addition of a small amount of PE to the C16 emulsion had minimal side effects on the apparent viscosity and droplet size, and 1% PE was recommended.

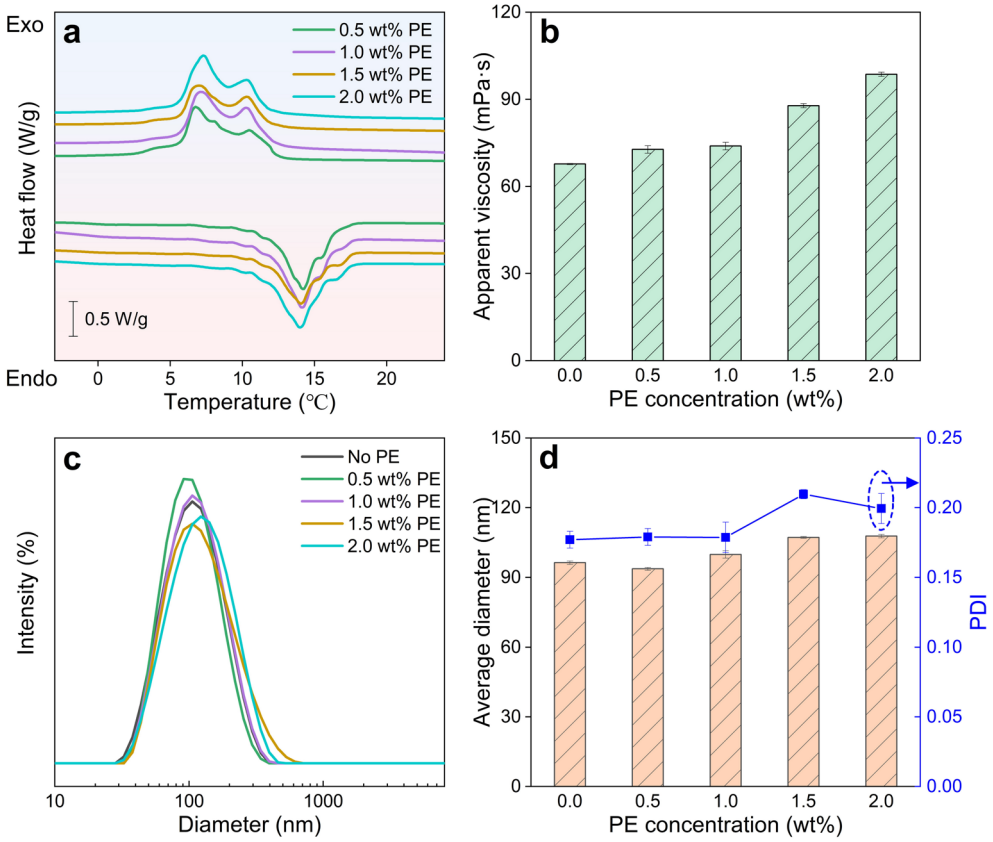

Fig. 3 Influence of PE concentration on properties of 20% C16 emulsion (10% surfactants) treated by ultrasound at 100% amplitude for 5 min: (a) DSC curves; (b) apparent viscosity; (c) droplet size distribution; (d) average diameter and PDI.

3.1.3 Effect of surfactant concentration on supercooling

To assess the influence of average diameter on supercooling suppression in 20% C16 emulsion, adjusting the surfactant concentration is the simplest and most efficient method to achieve various droplet sizes. Therefore, surfactant concentration was minimized to 2%, and different treatment periods with ultrasound at 100% amplitude were performed to ensure adequate emulsification. The resulting droplet size distribution characteristics and DSC curves are presented in **Fig. S2** (Supplementary data), which demonstrated that a longer treatment time of 10 minutes was preferable for surfactant concentrations between 2-4%, while 5 minutes remained suitable for intermediate surfactant concentrations.

Fig. 4a gives the droplet size distribution of 20% C16 emulsion with surfactant concentrations ranging from 2% to 10%. A monomodal distribution gradually shifted towards larger sizes but became sharper until the surfactant concentration decreased to 4%. At 2%

surfactants, the upper distribution limit abruptly exceeded 1000 nm, yielding a flat curve, which suggests that this concentration may be close to the minimum threshold needed to achieve a narrowly distributed C16 emulsion via ultrasonication. **Fig. 4b** presents the variations in average diameter and PDI as a function of surfactant concentration. It is evident that PDI continuously dropped from 0.18 to 0.15 and then increased to 0.25 at 2% surfactants. A relatively linear relationship was also obtained between average diameter and surfactant concentration. With an average diameter in the range of 96.4-256.3 nm, size-dependent freezing and melting behaviors can be well explored.

Fig. 4c-d depict the DSC freezing and melting curves of 20% C16 emulsion with various droplet sizes, using 2% PE-*b*-PEG and 1% PE, with detailed data provided in **Table 3**. It was discovered that the major freezing peak shifted with increasing droplet diameter, leading to the growth of the targeted peak ($T_{f,p} \approx 10$ ℃) and the diminishment of the undesired peak ($T_{f,p} = 6$-7 ℃). When the droplet size reached 256.3 nm, the DSC freezing curve nearly achieved the proposed ideal shape, validating the hypothesis that PE could promote C16 nucleation more effectively in larger droplets. Under these conditions, complete supercooling elimination was expected; however, ΔT only decreased to 3.7 ℃ (**Table 3**) due to size-dependent melting behaviors, which will be discussed later. Overall, in comparison to several previous studies of PCEs [27, 40, 41], where droplet size was large but supercooling remained unresolved with a high value ($\Delta T > 10$ ℃), the smaller diameter, lower ΔT, and well-controlled phase transition curves (almost single freezing and melting peaks) of the 20% C16 emulsion indicated novelty.

During the melting process, the main melting peak also experienced an evident shift with increasing average diameter, as reported in a previous study [35]. Specifically, the first melting peak ($T_{m,p} = 14.1$ ℃) was the largest for C16 droplets with a size of 96.4 nm, which disappeared as the droplet size increased to 256.3 nm, and the third melting peak ($T_{m,p} = 18.0$ ℃) emerged and became the primary peak (**Fig. 4d**). Assuming an infinite droplet size for bulk C16, $T_{m,p}$ was further raised to 19.9 ℃. In practice, size-dependent melting behavior for PCMs confined in nanoporous solids has been previously reviewed [42], and melting point depression showed a linear dependence on the reverse pore diameter of mesoporous substrates (2-50 nm) [43, 44],

usually explained by the Gibbs-Thomson thermodynamic equation [45].

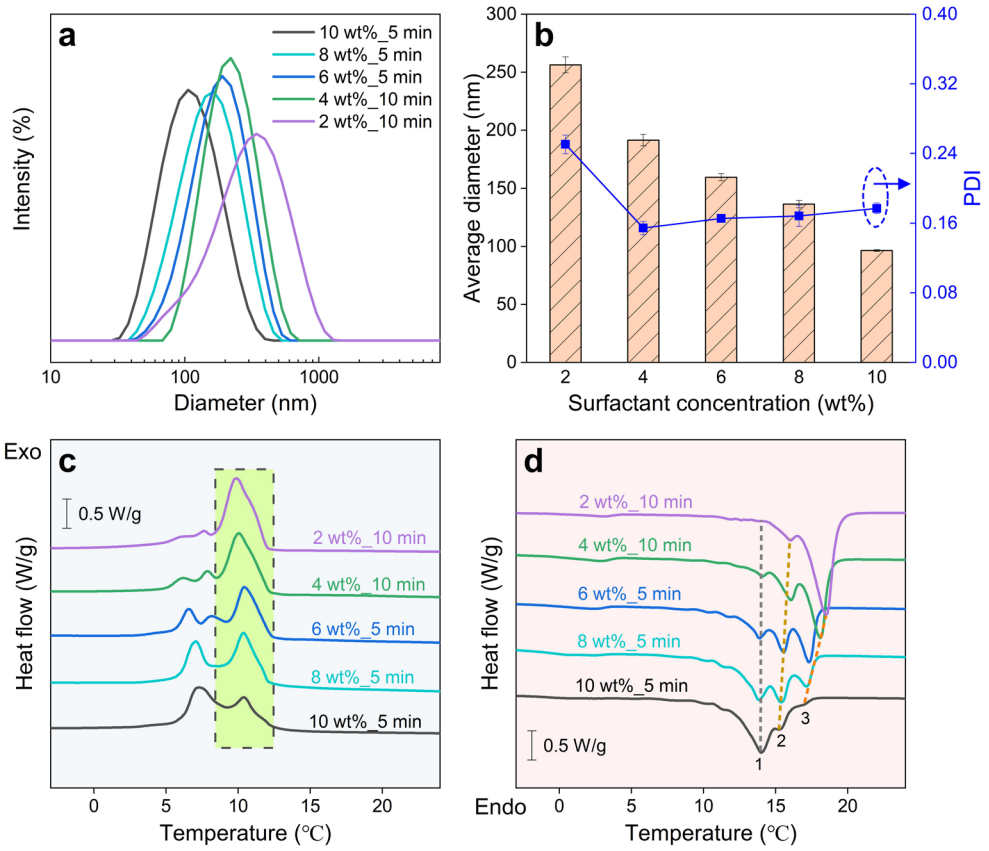

Fig. 4 Effects of surfactant concentration on properties of 20% C16 emulsion by adding 2% PE-*b*-PEG and 1% PE: (a) droplet size distribution; (b) average diameter and PDI; (c-d) DSC freezing and melting curves.

In this study, C16 spherical droplets can be considered as PCM in soft nanoconfinement by surfactant micelles, which could be helpful for understanding size-dependent melting point depression. Moreover, latent heat of C16 emulsion decreased in response to droplet size reduction. For instance, melting latent heat (ΔH_m) ranged from 44.3 J/g at 256.3 nm to 36.9 J/g at 96.4 nm, which could be interpreted similarly to the melting point. In short, attaining superior thermal properties and a long lifespan is the ultimate goal for the development of high-performance PCEs. The experimental results strongly suggest that size-dependent effects on the properties of PCEs must be thoroughly investigated, and equations for illustrating their relationships can be developed in future work to establish an interconnection of thermal properties and lifespan as a whole for PCEs. Effort was made to use more PE mass in the 20% C16 emulsion with 2% surfactants. It confirmed non concentration-dependent effect of PE on

the nucleation promotion of C16 droplets (**Fig. S3a**), and a mild diameter increment to 293.5 nm by adding 3% PE (**Fig. S3b**) also supported the opinion of a minor adverse effect of PE on the stability of the C16 emulsion.

Table 3 Effects of surfactant concentration on thermal properties of 20% C16 emulsion with the addition of 2% PE-*b*-PEG and 1% PE.

Surfactant	$T_{m,o}$ (°C)	$T_{m,p}$ (°C)	ΔH_m (J/g)	$T_{f,o}$ (°C)	$T_{f,p}$ (°C)	ΔH_f (J/g)	ΔT (°C)
10 wt%	11.6	1st: 14.1 2nd: 15.3	36.9	8.4	1st: 10.3 2nd: 7.2	36.8	3.2
8 wt%	13.6	1st: 13.8 2nd: 15.4 3rd: 17.2	39.2	12.2	1st: 10.3 2nd: 7.2	38.2	1.4
6 wt%	15.9	1st: 13.8 2nd: 15.6 3rd: 17.2	40.5	12.3	1st: 10.5 2nd: 8.2 3rd: 6.6	39.4	3.6
4 wt%	16.0	1st: 14.1 2nd: 16.1 3rd: 17.7	40.4	12.5	1st: 10.2 2nd: 7.8 3rd: 6.2	38.1	3.5
2 wt%	16.2	1st: 16.1 2nd: 18.0	44.3	12.5	1st: 10.4 2nd: 7.7	41.2	3.7

3.1.4 Assessment of long-term static stability

To evaluate static stability, the optimal C16 emulsion was stored in a glass bottle at room temperature for an extended period. After capturing a photo, the glass bottle gently rotated upside down a few times before taking the sample for characterization. As illustrated in **Fig. 5a**, the average diameter increased from 256.3 nm to 322.1 nm over three months, and no emulsion breakdown observed, as shown in the sample picture inserted in **Fig. 5b**. The DSC curves also indicated that the thermal properties of the optimal emulsion remained unchanged after long-term storage. Moreover, the freezing curve became narrower with the minor freezing peak at a lower temperature vanishing. The size increase may further intensity the role of PE in promoting C16 nucleation in larger droplets. However, the melting point remained unaffected, resulting in an unaltered ΔT. It can be hypothesized that the size-dependent effect on melting point depression might be negligible once the droplet size exceeds a certain threshold.

For comparison, the C16 emulsion with droplets at a diameter of 96.4 nm was characterized. The size increase to 119.8 nm caused variations in both melting and freezing

curves. The $T_{m,p}$ rose from 14.1 ℃ to 15.9 ℃ (**Fig. 5c**), supporting the assumption regarding a size threshold for melting point variation. In summary, additional experiments should be conducted on the same and different emulsions to clarify this. Furthermore, ΔT was larger over the three-month storage for the emulsion with a smaller size. With stability ensured, it is recommended that the droplet size be as large as possible to achieve high latent heat and less-varied phase change points.

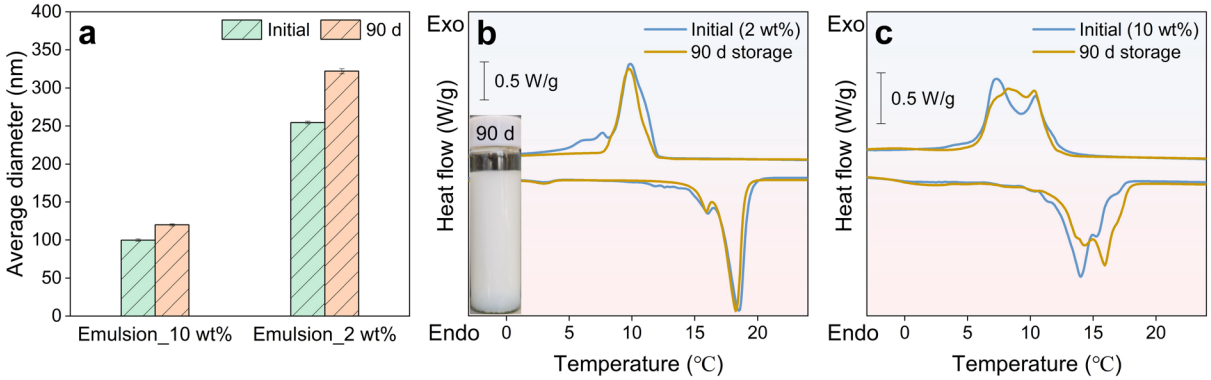

Fig. 5 Characteristics of 20% C16 emulsions with 2% or 10% surfactants during 90 days of static storage at room temperature: (a) average diameter; (b-c) DSC curves.

3.2 Supercooling suppression to other PCEs

The optimal chemical composition of 2% surfactants, 2% PE-*b*-PEG, and 1% PE, and ultrasonic treatment at 100% amplitude for 10 minutes, were attained based on a systematic evaluation of their effects on supercooling of C16 emulsion. These variables were applied to other PCEs with higher melting points, and the function of PE was clarified in OP28E emulsion. The emulsion with a larger diameter of 270.2 nm (**Fig. 6a**) exhibited a single main freezing peak with $T_{f,p}$ and ΔH_m at 23.1 ℃ and 39.8 J/g, respectively. A decrease in droplet diameter to 160 nm resulted in the freezing process being governed by two separate peaks (**Fig. 6b**). As a consequence, $T_{f,o}$ for the large freezing peak (ΔH_f = 23.5 J/g) was only 15.7 ℃, and ΔT was calculated to be 6.4 ℃, higher than the value (2.3 ℃) for the emulsion with a larger size. Moreover, the decrease in droplet diameter led to depressions in latent heat (from 38.9 to 35.1 J/g) and melting point (from 27.3 to 25.7 ℃), consistent with the trends observed in C16 emulsion.

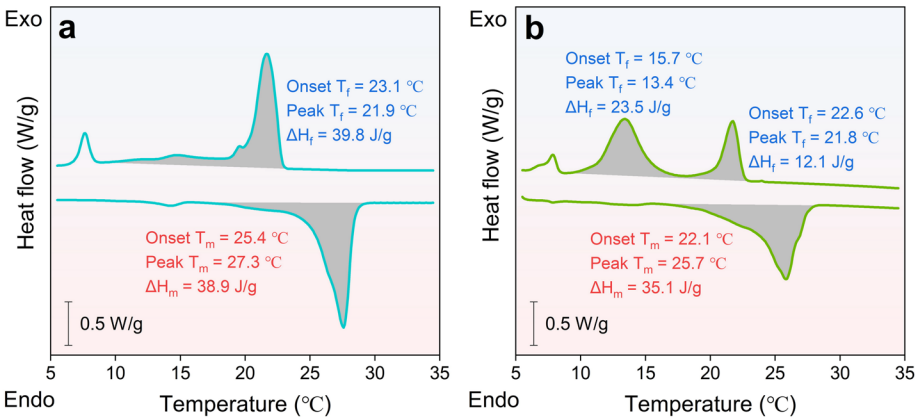

Fig. 6 DSC curves of 20% OP28E emulsion with surfactant concentration at (a) 2% or (b) 8%.

Fig. 7 displays the DSC curves of bulk PCMs and 20% PCEs, and **Table 4** summarizes the thermal property data. Comparing the DSC curves of the initial template of C16 and C16 emulsion (**Fig. 7a**) revealed that both melting and freezing peaks shifted after emulsification. As previously discussed, efforts were made to retain the desirable freezing peak, but $T_{f,p}$ of 10.4 ℃ was still lower than the bulk value of 15.9 ℃. Therefore, ΔT increased from 1.6 ℃ (bulk C16) to 3.7 ℃ (C16 emulsion). To the best of our knowledge, this could be the lowest ΔT reported in C16 emulsions with the nanoscale droplets. PE was then verified for reducing or even eliminating supercooling in other seven PCEs, as shown in **Fig. 7b-h**. The shift of melting and freezing peaks to a lower temperature range was also observed when other PCMs were emulsified into numerous small droplets in water. The selected PCMs exhibit the advantages of paraffins, such as a wide range of $T_{m,p}$ (20-70 ℃), high latent heat (up to ~270 J/g), and low supercooling (usually ΔT < 1.5 ℃), as shown in **Table 4**.

Rotator phases existed in bulk paraffins, including OP44E (**Fig. 7c**), C24 (**Fig. 7d**), C28 (**Fig. 7f**) and C32 (**Fig. 7h**), with two freezing peaks representing the transition from the liquid phase to the rotator phase (liquid-solid) and the solid-solid transition (rotator phase to crystal phase). More details about rotator phases of paraffins in bulk and in confinement can be found elsewhere [46]. For PCMs with rotator phases, the emulsion counterparts exhibited a significantly improved latent heat proportion for the peak of liquid-solid transition, and supercooling in these four PCEs was essentially addressed. In other paraffins (OP28E, Sal52 and OP65E), the corresponding PCEs displayed a single freezing curve with ΔT at around 2.5 ℃.

Based on these experimental results, it can be concluded that PE can eliminate or significantly reduce supercooling in paraffin emulsions with a broad melting point range. This achievement represents a significant breakthrough against the persistent and troublesome issue of supercooling in PCEs.

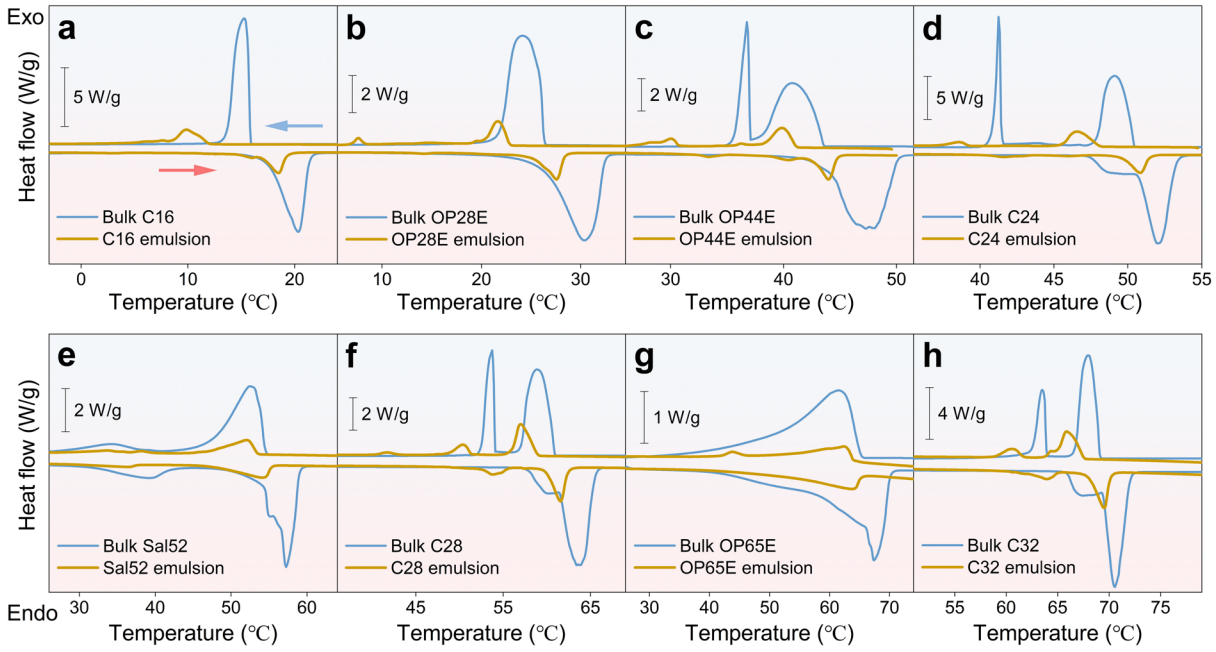

Fig. 7 DSC curves of various PCMs and corresponding 20% PCEs: (a) C16; (b) OP28E; (c) OP44E; (d) C24; (e) Sal52; (f) C28; (g) OP65E; (h) C32.

The confinement of PCM droplets by surfactant micelles can result in lower latent heat compared to the theoretical values of bulk PCMs, as supported by the major PCMs listed in **Table 4**. Interestingly, two high-melting alkanes exhibited an inverse trend with higher latent heat, i.e., ~57 J/g versus ~52 J/g (20% bulk C28), and ~60 J/g versus ~51 J/g (20% bulk C32). Multiple assumptions, such as the interaction between PE and high-melting alkanes and the variation of rotator phases in bulk and in confinement, should be further investigated.

Table 4 Thermal properties of PCMs and the related PCEs.

PCM	Status	$T_{m,o}$ (°C)	$T_{m,p}$ (°C)	ΔH_m (J/g)	$T_{f,o}$ (°C)	$T_{f,p}$ (°C)	ΔH_f (J/g)	ΔT (°C)
C16	bulk	17.5	19.9	225.2	15.9	15.9	226.6	1.6
	emul.	16.2	18.0	44.3	12.5	10.4	41.2	3.7
OP28E	bulk	26.1	29.5	231.9	26.5	25.2	233.4	0.4
	emul.	25.4	27.3	38.9	23.1	21.9	39.8	2.3

OP44E	bulk	43.5	46.0	240.8	43.4	1^{st}: 40.8 2^{nd}: 37.2	243.2	0.1
	emul.	42.4	43.7	41.3	41.2	1^{st}: 40.0 2^{nd}: 30.2	42.1	1.2
C24	bulk	50.3	51.3	270.7	50.5	1^{st}: 49.7 2^{nd}: 42.3	266.8	0.2
	emul.	49.1	50.5	45.5	48.1	1^{st}: 46.8 2^{nd}: 38.7	45.8	1.0
Sal52	bulk	53.4	57.3	178.2	54.6	52.6	175.5	1.2
	emul.	51.3	53.8	32.9	53.7	52.3	31.2	2.4
C28	bulk	60.8	62.3	258.7	61.0	1^{st}: 59.9 2^{nd}: 54.9	257.8	0.2
	emul.	59.8	61.1	57.4	59.0	1^{st}: 57.4 2^{nd}: 51.4	56.6	0.8
OP65E	bulk	63.9	66.8	177.6	65.2	62.0	175.9	1.3
	emul.	61.5	63.6	31.1	64.1	62.5	30.5	2.6
C32	bulk	69.3	70.7	258.8	69.2	1^{st}: 68.6 2^{nd}: 63.6	248.4	0.1
	emul.	67.8	69.1	59.2	67.6	1^{st}: 66.2 2^{nd}: 60.7	60.7	0.2

For the preliminary evaluation of service life, one-month storage at room temperature was conducted. **Fig. 8a-g** shows the DSC curves of 20% PCEs before and after the static evaluation in a glass bottle, where both melting and freezing curves highly overlapped, except for the emulsions of OP28E and C32 with a minor shift to about 0.5 ℃ higher. As seen in **Fig. 8h**, the average diameter of PCEs upon preparation generally increased with the $T_{m,p}$ rise of PCMs, and the largest diameter was reached 468.2 nm for the OP65E emulsion. Over the 30-day storage, the diameter increment was only 10-20 nm, indicating good static stability. Therefore, it is worth conducing an evaluation of long-term dynamic stability of PCEs, and Sal52 emulsion was selected as the representative for two reasons. Firstly, Sal52 was the most economical option, and low cost is crucial of large-scale applications. Secondly, the relatively high working temperature over $T_{m,p}$ of the Sal52 emulsion can profoundly accelerate the emulsion breakdown. If the Sal52 emulsion can survive under the simulated conditions, it would be reasonable to expect that other PCEs with a lower $T_{m,p}$ can also have a long service life. Furthermore, PCEs with a $T_{m,p}$ less than 50 ℃ are the most common option in research, and the acquired lifespan in the present study should be meaningful and feasible for potential applications of PCEs, such as in thermal management systems.

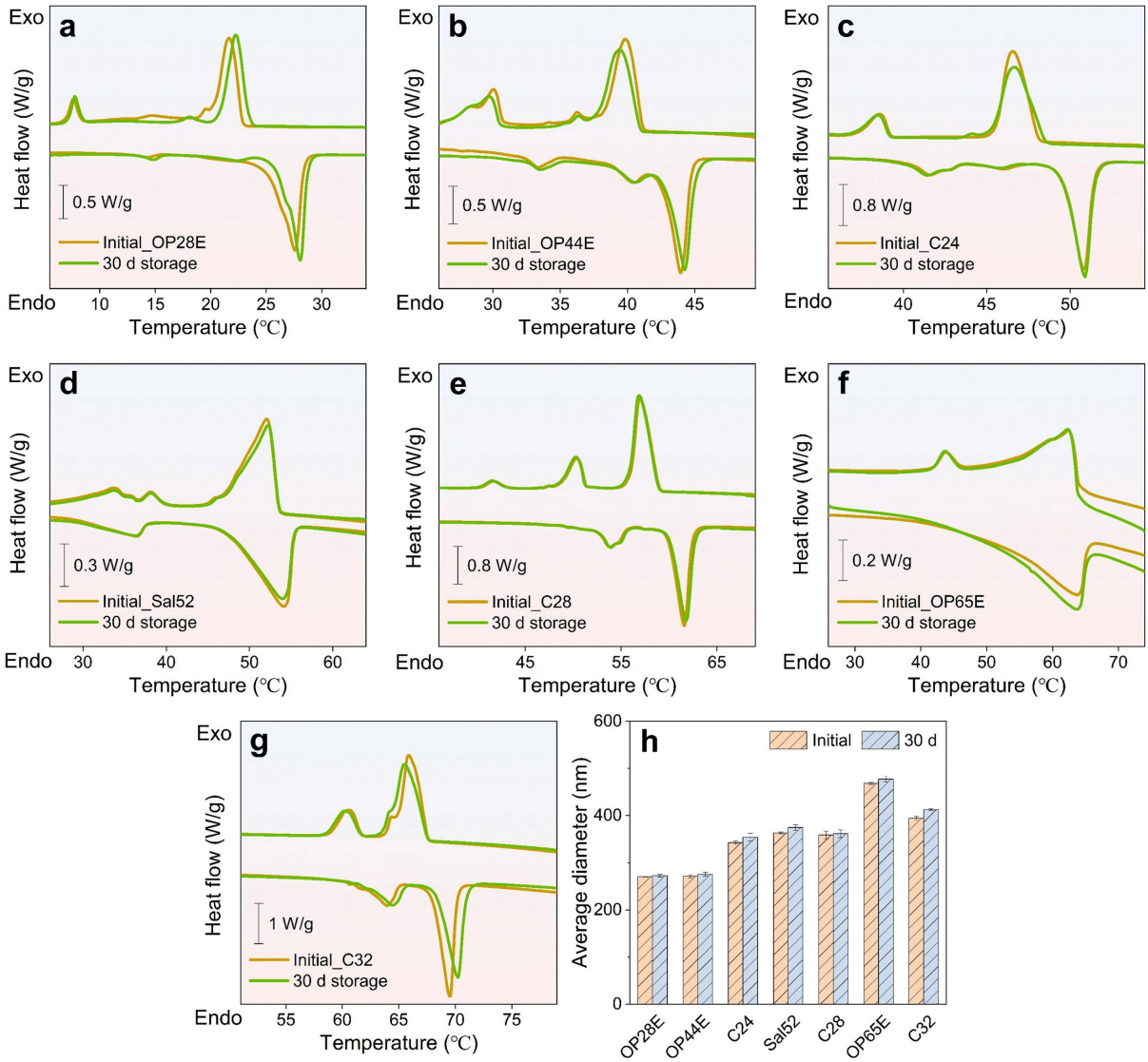

Fig. 8 Stability of 20% PCEs at 25 ℃ over 30 days: (a-g) DSC curves; (h) average diameter.

3.3 Assessment of long-term dynamic stability

The dynamic stability of the 20% Sal52 emulsion was evaluated using a custom-built lab-scale test rig (**Fig. 9a**), which included three tanks for heating, cooling, and storage, two copper coils (10 mm outer diameter and 4.5 m total length) submerged in hot (65 ℃) and cold (22 ℃) water baths for heat exchange, and an electromagnetic diaphragm metering pump for circulating the emulsion through rubber pipes with a 10 mm inner diameter. The volume of the cold water bath was 6.5 L, with fresh tap water overflowing to maintain a constant temperature. By adjusting the temperature of the electro-thermostatic water bath, filling it with 10 L of water, and controlling the flow rate through the metering pump, the emulsion could circulate and undergo complete melting and freezing processes. The Sal52 emulsion production was limited

to 200 g per batch due to the limitation of probe-type sonicator in laboratory. Five batches were prepared, yielding a total emulsion volume of approximately 1 L for rig operation. As demonstrated in the Supplementary data, subjecting a 10-fold larger emulsion mass to ultrasonication did not lead to any alteration in thermal properties (**Fig. S4a**). Moreover, the average diameter of the droplets only exhibited a slight increase from 363.3 nm to 374.1 nm, while maintaining an overlapped monoidal droplet size distribution, as presented in **Fig. S4b**. The Sal52 emulsion was pumped at flow rate of 6 L/h for 10 hours daily, totaling 250 hours per month. During a 10-h operation, the emulsion temperatures exiting the heating tank (T_1) and within the storage tank (T_2) were measured using two thermocouples and recorded by a data logger (**Fig. 9b**). The minor temperature fluctuations ($T_1 \approx 60$ °C; $T_2 \approx 26.5$ °C) suggested that the Sal52 emulsion could fully melt and solidify when pumped through the heating and cooling tanks. The emulsion was operated for six months, undergoing a total of 9000 thermal cycles. This marks the first time PCEs have been evaluated with such a long duration and a high number of thermal cycles.

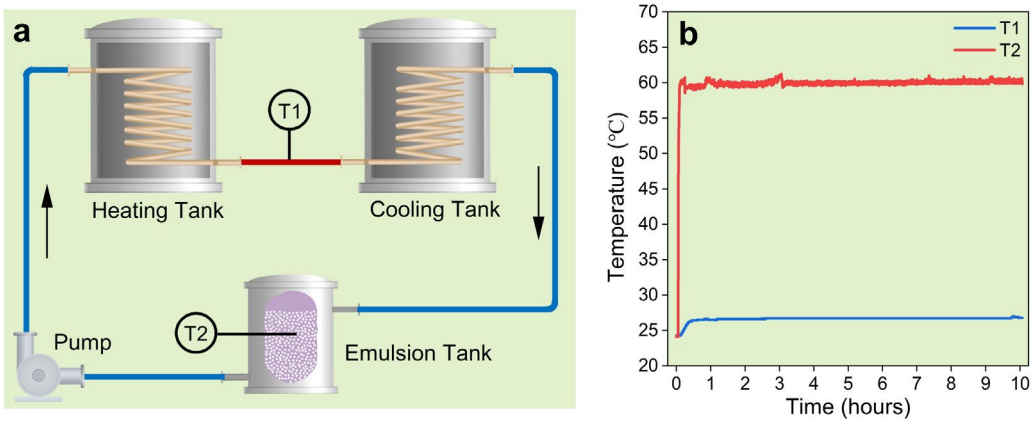

Fig. 9 the test rig for dynamic stability evaluation of Sal52 emulsion: (a) schematic diagram; (b) temperature variation.

Fig. 10 illustrates the properties of the 20% Sal52 emulsion after a six-month dynamic stability assessment. As depicted in **Fig. 10a**, the average diameter was determined for every 300 thermal cycles, revealing a periodic fluctuation with a small difference (~55 nm) between the largest and smallest diameter. Ultimately, the diameter slightly increased from 374.1 nm to 393.4 nm after 9000 thermal cycles. Conversely, the droplet size distribution became trimodal

and wider (**Fig. 10b**), and the PDI was notably increased from 0.13 to 0.41. Coalescence was likely the primary mechanism for emulsion destabilization associated with the change in droplet size distribution. A similar trend was also documented in reference [47], where PCEs underwent 100 thermal cycles in a cylindrical cup while being subjected to a constant shear rate of 100 s^{-1} to simulate emulsion flow in pipes.

After the test, approximately 0.85 L of Sal52 emulsion was retrieved from the rig, and the inset image in **Fig. 10b** confirmed that no emulsion breakdown was observed over 9000 thermal cycles in six months. Furthermore, an additional six months of storage was carried out, showing in **Fig. S5**, from which no obvious breakdown was observed. The morphologies of the Sal52 emulsion before and after thermal cycling are shown in **Fig. 10c-d**, which generally agree with the DLS measurements. Initially, the emulsion displayed a uniform distribution with small particle sizes. Collisions between droplets during the heating process or particles during the cooling process resulted in the formation of larger and smaller droplets, respectively, as evidenced by the trimodal droplet distribution and increased PDI. **Fig. 10e-f** present the DSC freezing and melting curves, which reveal no obvious shift in phase transition peaks for the Sal52 emulsion after 9000 thermal cycles. This further supports the innovation of the developed PCEs. Specifically, the latent heat was slightly reduced to around 29 J/g after thermal cycling, as illustrated in **Fig. 10g**, and both melting and freezing points decreased by around 1 °C (**Fig. 10h**), resulting in a nearly constant supercooling degree. The minimal supercooling and extended service life make the PCEs a promising coolant for use in thermal management and TES systems. Moreover, by incorporating additional functional additives such as two-dimension transition metal carbide/nitride (MXene) materials [48] into the PCEs, a high photothermal conversion efficiency can be achieved for broader applications.

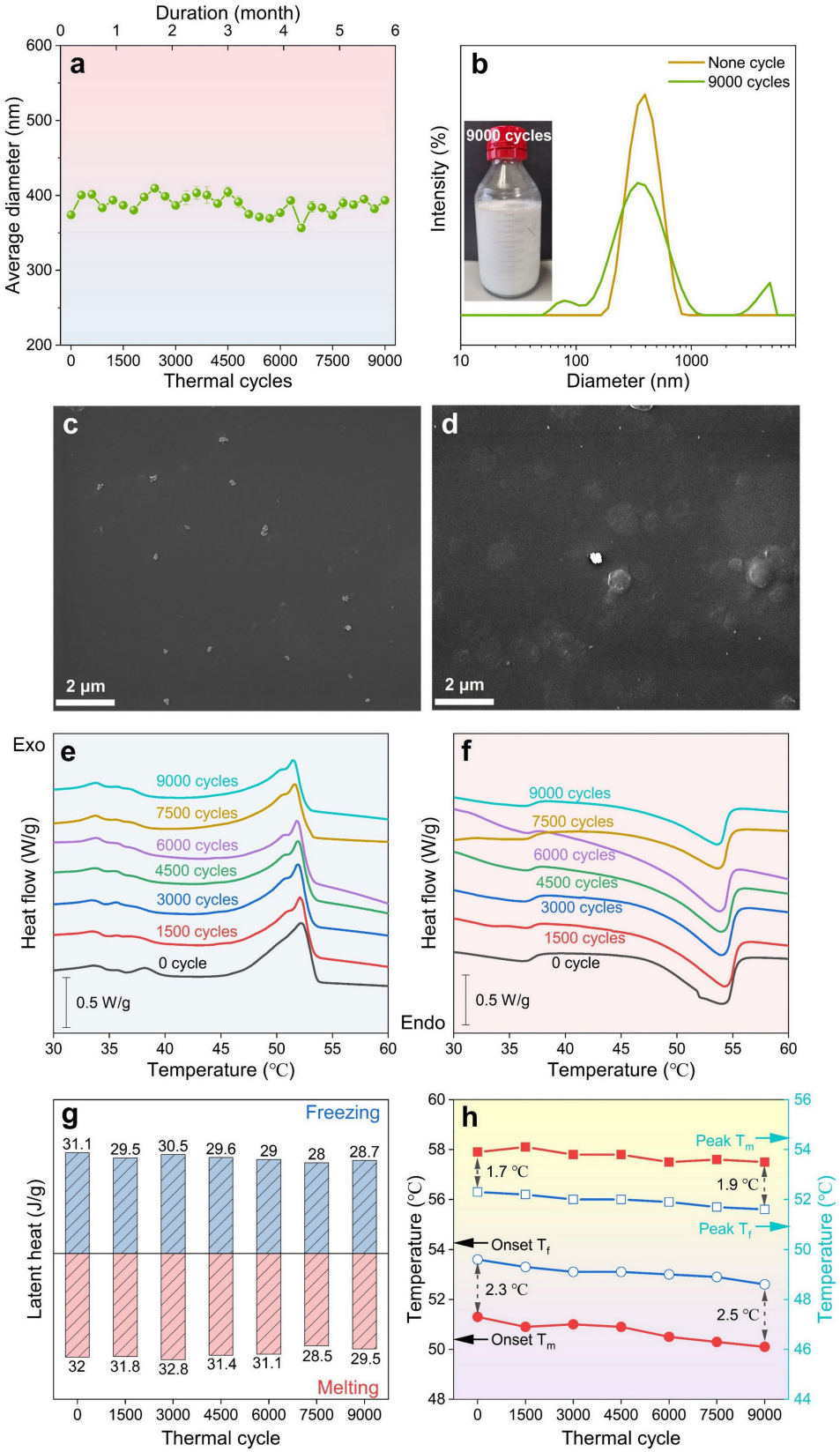

Fig. 10 The properties of 20% Sal52 emulsion over 9000 thermal cycles: (a) average diameter; (b) droplet size distribution; (c-d) morphologies before and after thermal cycling; (e-f) DSC freezing and melting curves; (g) latent heat; (h) phase transition points.

4. Conclusions

The present study developed an effective strategy for overcoming the high supercooling problem in phase change emulsions (PCEs) of small particle or droplet size. The essential idea was to induce simultaneous nucleation in the core of PCEs with a low molecular weight polyethylene (PE) and at the PCE-water interface with a diblock copolymer. The chemical compositions and the effects of ultrasonication were optimized to minimize the supercooling. High-power ultrasound was a crucial factor for the effectiveness of PE in nucleation within the PCEs of small droplet size. A larger droplet (e.g. 256.3 nm) could achieve near-singular melting and freezing peaks with a low supercooling degree (3.7 °C). The developed strategy was proven effective for a wide range of paraffin emulsions, achieving minimal supercooling degrees. The optimized PCE formulation has been scaled up and applied to a rig successful for a long period of operation through many thermal cycles. Therefore, the new strategy may be feasible and applicable for development of high-performance PCEs with a broad melting point range, minimal supercooling degree, and long-service life for large-scale applications. However, further research is needed to investigate the decreases in latent heat and melting point as the droplet size decreases.

Acknowledgments

This work was supported financially by the Environment and Conservation Fund (ECF 588 Project 53/2018) and by the Hong Kong Polytechnic University.

References

[1] P. Singh, R.K. Sharma, A.K. Ansu, R. Goyal, A. Sarı, V.V. Tyagi, A comprehensive review on development of eutectic organic phase change materials and their composites for low and medium range thermal energy storage applications, Solar Energy Materials and Solar Cells 223 (2021) 110955. https://doi.org/10.1016/j.solmat.2020.110955

[2] K. Matuszek, M. Kar, J.M. Pringle, D.R. MacFarlane, Phase Change Materials for Renewable Energy Storage at Intermediate Temperatures, Chemical Reviews 123(1) (2023) 491-514. https://doi.org/10.1021/acs.chemrev.2c00407

[3] C. Zhou, S. Wu, Medium- and high-temperature latent heat thermal energy storage: Material database, system review, and corrosivity assessment, International Journal of Energy Research 43(2) (2019) 621-661. https://doi.org/10.1002/er.4216

[4] G. Wang, Z. Tang, Y. Gao, P. Liu, Y. Li, A. Li, X. Chen, Phase Change Thermal Storage Materials for Interdisciplinary Applications, Chemical Reviews (2023). https://doi.org/10.1021/acs.chemrev.2c00572

[5] E.M. Shchukina, M. Graham, Z. Zheng, D.G. Shchukin, Nanoencapsulation of phase change materials for advanced thermal energy storage systems, Chemical Society Reviews 47(11) (2018) 4156-4175. https://doi.org/10.1039/C8CS00099A

[6] X. Huang, C. Zhu, Y. Lin, G. Fang, Thermal properties and applications of microencapsulated PCM for thermal energy storage: A review, Applied Thermal Engineering 147 (2019) 841-855. https://doi.org/10.1016/j.applthermaleng.2018.11.007

[7] Z. Chen, J. Zhang, S. Deng, M. Hou, X. Zhang, Z. Jiang, N.-C. Lai, Morphology-controlled synthesis of Cu2O encapsulated phase change materials: Photothermal conversion and storage performance in visible light regime, Chemical Engineering Journal 454 (2023) 140089. https://doi.org/10.1016/j.cej.2022.140089

[8] M. Jurkowska, I. Szczygieł, Review on properties of microencapsulated phase change materials slurries (mPCMS), Applied Thermal Engineering 98 (2016) 365-373. https://doi.org/10.1016/j.applthermaleng.2015.12.051

[9] V. Soni, S. Saber, H. McPhee, J. Riordon, M. Zargartalebi, M. Holmes, M. Toews, D. Sinton, Evaluation of a Microencapsulated Phase Change Slurry for Subsurface Energy Recovery, Energy & Fuels 35(12) (2021) 10293-10302. https://doi.org/10.1021/acs.energyfuels.1c00972

[10] B. Xu, C. Chen, J. Zhou, Z. Ni, X. Ma, Preparation of novel microencapsulated phase change material with Cu-Cu2O/CNTs as the shell and their dispersed slurry for direct absorption solar collectors, Solar Energy Materials and Solar Cells 200 (2019) 109980. https://doi.org/10.1016/j.solmat.2019.109980

[11] R. Pakrouh, M.J. Hosseini, R. Bahrampoury, A.A. Ranjbar, S.M. Borhani, Cylindrical battery thermal management based on microencapsulated phase change slurry, Journal of

505 Energy Storage 40 (2021) 102602. https://doi.org/10.1016/j.est.2021.102602
506 [12] A.H. Eisapour, M. Eisapour, M.J. Hosseini, A.H. Shafaghat, P. Talebizadeh Sardari, A.A.
507 Ranjbar, Toward a highly efficient photovoltaic thermal module: Energy and exergy analysis,
508 Renewable Energy 169 (2021) 1351-1372. https://doi.org/10.1016/j.renene.2021.01.110
509 [13] H. Kazemi-Varnamkhasti, I. Khazaee, M. Ameri, D. Toghraie, Heat storage and increasing
510 the rate of heat transfer in polymer electrolyte membrane fuel cell by adding nano-encapsulated
511 phase change material to water in the cooling process, Journal of Energy Storage 59 (2023)
512 106497. https://doi.org/10.1016/j.est.2022.106497
513 [14] S. Mo, J. Ye, L. Jia, Y. Chen, Properties and performance of hybrid suspensions of
514 MPCM/nanoparticles for LED thermal management, Energy 239 (2022) 122650.
515 https://doi.org/10.1016/j.energy.2021.122650
516 [15] M. Graham, J. Smith, M. Bilton, E. Shchukina, A.A. Novikov, V. Vinokurov, D.G.
517 Shchukin, Highly Stable Energy Capsules with Nano-SiO2 Pickering Shell for Thermal Energy
518 Storage and Release, ACS Nano 14(7) (2020) 8894-8901.
519 https://doi.org/10.1021/acsnano.0c03706
520 [16] Z. Sun, L. Zhao, H. Wan, H. Liu, D. Wu, X. Wang, Construction of polyaniline/carbon
521 nanotubes-functionalized phase-change microcapsules for thermal management application of
522 supercapacitors, Chemical Engineering Journal 396 (2020) 125317.
523 https://doi.org/10.1016/j.cej.2020.125317
524 [17] Z. Zhang, Z. Zhang, T. Chang, J. Wang, X. Wang, G. Zhou, Phase change material
525 microcapsules with melamine resin shell via cellulose nanocrystal stabilized Pickering
526 emulsion in-situ polymerization, Chemical Engineering Journal 428 (2022) 131164.
527 https://doi.org/10.1016/j.cej.2021.131164
528 [18] A. Mustapha, Y. Wang, Y. Ding, Y. Li, Supercooling elimination of cryogenic-temperature
529 microencapsulated phase change materials (MPCMs) and the rheological behaviors of their
530 suspension, Journal of Materials Research and Technology 21 (2022) 2277-2295.
531 https://doi.org/10.1016/j.jmrt.2022.10.010
532 [19] Y. Zhu, Y. Qin, S. Liang, K. Chen, C. Tian, J. Wang, X. Luo, L. Zhang, Graphene/SiO2/n-

533 octadecane nanoencapsulated phase change material with flower like morphology, high thermal
534 conductivity, and suppressed supercooling, Applied Energy 250 (2019) 98-108.
535 https://doi.org/10.1016/j.apenergy.2019.05.021
536 [20] Z. Qiu, Y. Zhou, Y. Yao, F. Liu, R. Guo, Modification of microencapsulated phase change
537 materials(MPCMs) by synthesizing graphene quantum dots(GQDs) and nano-aluminum for
538 energy storage and heat transfer applications, Energy 181 (2019) 1331-1338.
539 https://doi.org/10.1016/j.energy.2019.05.080
540 [21] Z. Zhang, Y. Yuan, N. Zhang, X. Cao, Experimental investigation on thermophysical
541 properties of capric acid–lauric acid phase change slurries for thermal storage system, Energy
542 90 (2015) 359-368. https://doi.org/10.1016/j.energy.2015.06.129
543 [22] D. Cabaleiro, F. Agresti, L. Fedele, S. Barison, C. Hermida-Merino, S. Losada-Barreiro, S.
544 Bobbo, M.M. Piñeiro, Review on phase change material emulsions for advanced thermal
545 management: Design, characterization and thermal performance, Renewable and Sustainable
546 Energy Reviews 159 (2022) 112238. https://doi.org/10.1016/j.rser.2022.112238
547 [23] L. Liu, J. Niu, J.-Y. Wu, Improving energy efficiency of photovoltaic/thermal systems by
548 cooling with PCM nano-emulsions: An indoor experimental study, Renewable Energy 203
549 (2023) 568-582. https://doi.org/10.1016/j.renene.2022.12.090
550 [24] Y. Wang, J. Luo, S. Wang, Q. Ma, D. Zou, Shape-stabilized phase change material with
551 internal coolant channel coupled with phase change emulsion for power battery thermal
552 management, Chemical Engineering Journal 438 (2022) 135648.
553 https://doi.org/10.1016/j.cej.2022.135648
554 [25] M. Biedenbach, L. Poetzsch, S. Gschwander, Characterization of an n-octadecane PCS in
555 a 0.5 m^3 storage tank test facility, International Journal of Refrigeration 104 (2019) 76-83.
556 https://doi.org/10.1016/j.ijrefrig.2019.04.028
557 [26] G. Zhang, Z. Yu, G. Cui, B. Dou, W. Lu, X. Yan, Fabrication of a novel nano phase change
558 material emulsion with low supercooling and enhanced thermal conductivity, Renewable
559 Energy 151 (2020) 542-550. https://doi.org/10.1016/j.renene.2019.11.044
560 [27] T. Kawanami, K. Togashi, K. Fumoto, S. Hirano, P. Zhang, K. Shirai, S. Hirasawa,

561 Thermophysical properties and thermal characteristics of phase change emulsion for thermal
562 energy storage media, Energy 117 (2016) 562-568.
563 https://doi.org/10.1016/j.energy.2016.04.021
564 [28] L. Liu, J. Niu, J.-Y. Wu, Formulation of highly stable PCM nano-emulsions with reduced
565 supercooling for thermal energy storage using surfactant mixtures, Solar Energy Materials and
566 Solar Cells 223 (2021) 110983. https://doi.org/10.1016/j.solmat.2021.110983
567 [29] D. López-Pedrajas, A.M. Borreguero, F.J. Ramos, J.F. Rodríguez, M. Jiménez-Vázquez,
568 M. Carmona, Influence of the dispersion characteristics for producing thermoregulating nano
569 phase change slurries, Chemical Engineering Journal 452 (2023) 139034.
570 https://doi.org/10.1016/j.cej.2022.139034
571 [30] G. Hagelstein, S. Gschwander, Reduction of supercooling in paraffin phase change slurry
572 by polyvinyl alcohol, International Journal of Refrigeration 84 (2017) 67-75.
573 https://doi.org/10.1016/j.ijrefrig.2017.08.016
574 [31] T. Morimoto, H. Kumano, Nucleation promoting effect of fat shell on phase change
575 material particles dispersed in an emulsion for thermal energy storage medium, Journal of
576 Energy Storage 31 (2020) 101637. https://doi.org/10.1016/j.est.2020.101637
577 [32] X. Zhang, J. Niu, S. Zhang, J.-Y. Wu, PCM in Water Emulsions: Supercooling Reduction
578 Effects of Nano-Additives, Viscosity Effects of Surfactants and Stability, Advanced
579 Engineering Materials 17(2) (2015) 181-188. https://doi.org/10.1002/adem.201300575
580 [33] S. Barison, D. Cabaleiro, S. Rossi, A. Kovtun, M. Melucci, F. Agresti, Paraffin–graphene
581 oxide hybrid nano emulsions for thermal management systems, Colloids and Surfaces A:
582 Physicochemical and Engineering Aspects 627 (2021) 127132.
583 https://doi.org/10.1016/j.colsurfa.2021.127132
584 [34] D. Cabaleiro, F. Agresti, S. Barison, M.A. Marcos, J.I. Prado, S. Rossi, S. Bobbo, L. Fedele,
585 Development of paraffinic phase change material nanoemulsions for thermal energy storage
586 and transport in low-temperature applications, Applied Thermal Engineering 159 (2019)
587 113868. https://doi.org/10.1016/j.applthermaleng.2019.113868
588 [35] L. Liu, X. Zhang, H. Liang, J. Niu, J.-Y. Wu, Cooling storage performance of a novel phase

589 change material nano-emulsion for room air-conditioning in a self-designed pilot thermal
590 storage unit, Applied Energy 308 (2022) 118405.
591 https://doi.org/10.1016/j.apenergy.2021.118405
592 [36] J. Feng, J. Huang, Z. Ling, X. Fang, Z. Zhang, Performance enhancement of a photovoltaic
593 module using phase change material nanoemulsion as a novel cooling fluid, Solar Energy
594 Materials and Solar Cells 225 (2021) 111060. https://doi.org/10.1016/j.solmat.2021.111060
595 [37] L. Liu, J. Niu, J.-Y. Wu, Development of highly stable paraffin wax/water phase change
596 material nano-emulsions as potential coolants for thermal management, Solar Energy Materials
597 and Solar Cells 252 (2023) 112184. https://doi.org/10.1016/j.solmat.2023.112184
598 [38] T. Kousksou, T. El Rhafiki, M. Mahdaoui, P. Bruel, Y. Zeraouli, Crystallization of
599 supercooled PCMs inside emulsions: DSC applications, Solar Energy Materials and Solar Cells
600 107 (2012) 28-36. https://doi.org/10.1016/j.solmat.2012.07.023
601 [39] F.C. Meldrum, C. O'Shaughnessy, Crystallization in Confinement, Advanced Materials
602 32(31) (2020) 2001068. https://doi.org/10.1002/adma.202001068
603 [40] J. Chen, P. Zhang, Preparation and characterization of nano-sized phase change emulsions
604 as thermal energy storage and transport media, Applied Energy 190 (2017) 868-879.
605 https://doi.org/10.1016/j.apenergy.2017.01.012
606 [41] F. Wang, J. Cao, Z. Ling, Z. Zhang, X. Fang, Experimental and simulative investigations
607 on a phase change material nano-emulsion-based liquid cooling thermal management system
608 for a lithium-ion battery pack, Energy 207 (2020) 118215.
609 https://doi.org/10.1016/j.energy.2020.118215
610 [42] S. Zhang, Z. Wang, Thermodynamics behavior of phase change latent heat materials in
611 micro-/nanoconfined spaces for thermal storage and applications, Renewable and Sustainable
612 Energy Reviews 82 (2018) 2319-2331. https://doi.org/10.1016/j.rser.2017.08.080
613 [43] M.R. Pallaka, D.K. Unruh, S.L. Simon, Melting behavior of n-alkanes in anodic aluminum
614 oxide (AAO) nanopores using Flash differential scanning calorimetry, Thermochimica Acta
615 663 (2018) 157-164. https://doi.org/10.1016/j.tca.2018.01.016
616 [44] X. Wang, Y. Wei, D. Zhang, X. Lan, F. Han, X.Z. Lan, Phase behaviors of n-octacosane in

nanopores: Role of pore size and morphology, Thermochimica Acta 690 (2020) 178687. https://doi.org/10.1016/j.tca.2020.178687

[45] C.L. Jackson, G.B. McKenna, The melting behavior of organic materials confined in porous solids, The Journal of Chemical Physics 93(12) (1990) 9002-9011. https://doi.org/10.1063/1.459240

[46] D. Cholakova, N. Denkov, Rotator phases in alkane systems: In bulk, surface layers and micro/nano-confinements, Advances in Colloid and Interface Science 269 (2019) 7-42. https://doi.org/10.1016/j.cis.2019.04.001

[47] S. Gschwander, S. Niedermaier, S. Gamisch, M. Kick, F. Klünder, T. Haussmann, Storage Capacity in Dependency of Supercooling and Cycle Stability of Different PCM Emulsions, Applied Sciences, 2021.

[48] F. Wang, J. Guo, S. Li, Y. Wang, X. Hu, Z. Li, Y. Shen, C. Li, Facile self-assembly approach to construct a novel MXene-decorated nano-sized phase change material emulsion for thermal energy storage, Ceramics International 48(4) (2022) 4722-4731. https://doi.org/10.1016/j.ceramint.2021.11.008

Appendix A. Supplementary data

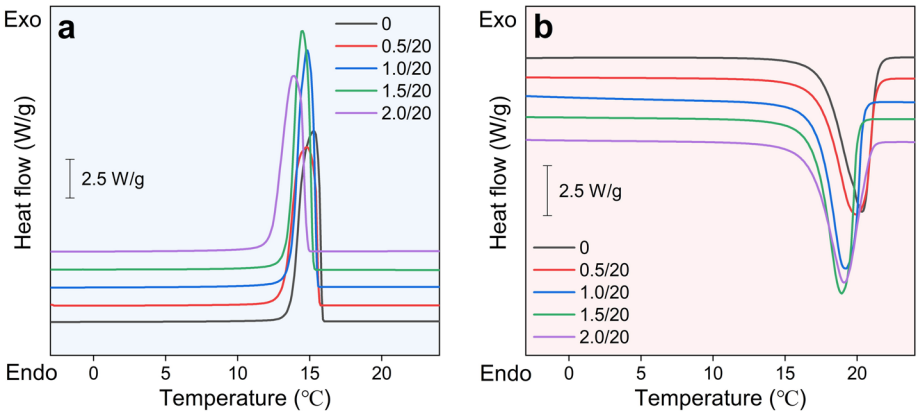

Fig. S1 DSC freezing (a) and melting (b) curves of bulk C16 by adding PE with its mass ratio to bulk C16 at (0.5-2.0)/20.

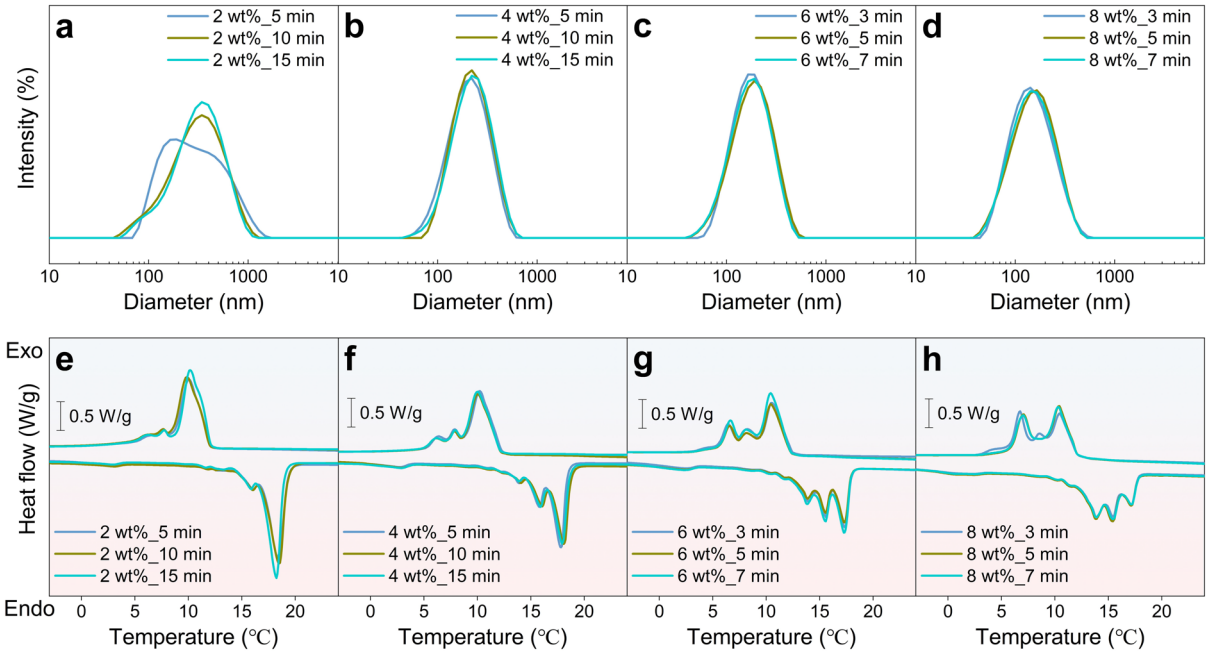

Fig. S2 Effects of ultrasound time (100% amplitude) on properties of 20% C16 emulsion by varying surfactant concentration in 2-8%: (a-d) droplet size distribution; (e-h) DSC curves.

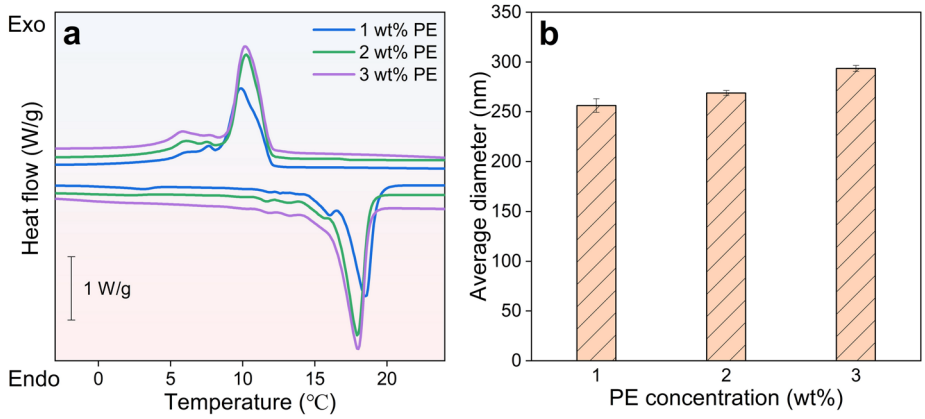

641

642 **Fig. S3** Effects of PE concentration on properties of 20% C16 emulsion (2% surfactants) treated

643 by ultrasound at 100% amplitude for 10 min: (a) DSC curves; (b) average diameter.

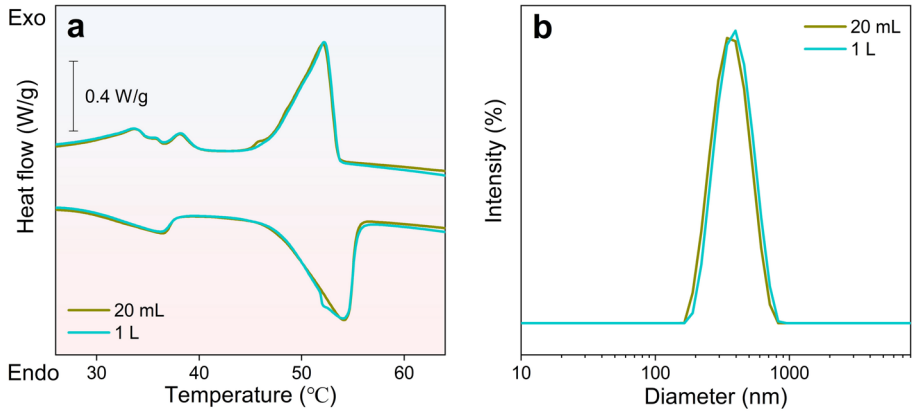

644

645 **Fig. S4** Comparisons between 20% Sal52 emulsions produced in small and large volumes: (a)

646 DSC curves; (b) droplet size distribution.

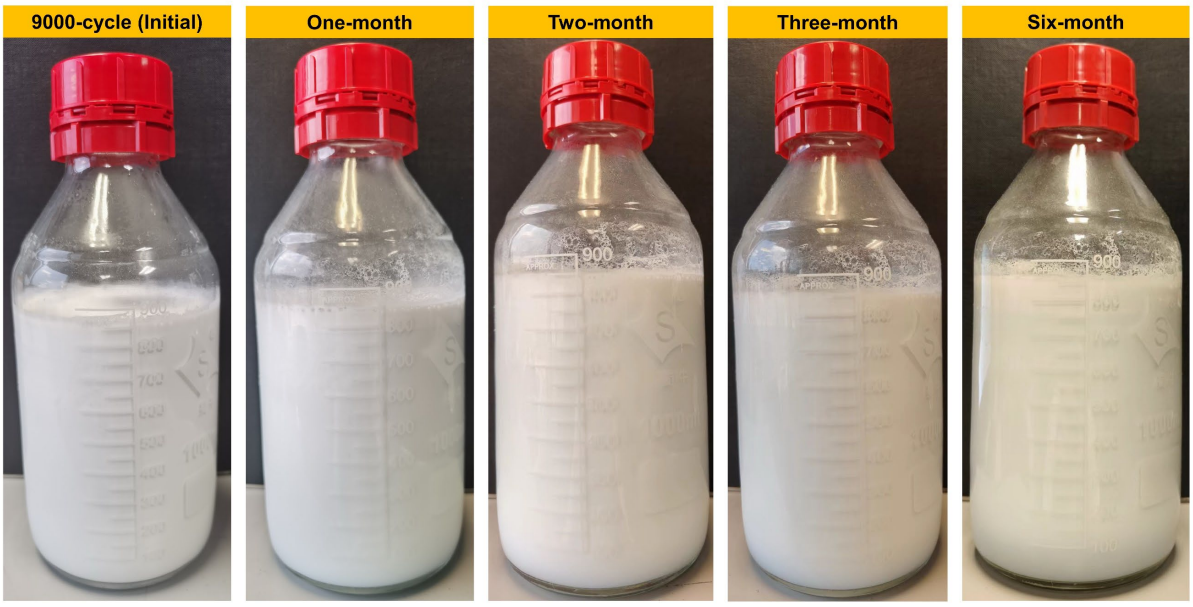

647

648 **Fig. S5** Photographs of 20% Sal52 emulsion after 9000 thermal cycles followed by storage over

649 six months at room temperature.